Biomaterials 305 (2024) 122426

Contents lists available at ScienceDirect

Biomaterials

journal homepage: www.elsevier.com/locate/biomaterials

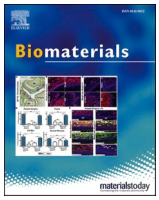

Stretch-injury promotes microglia activation with enhanced phagocytic and synaptic stripping activities

Anthony Procès [a,b], Yeranddy A. Alpizar [c], Sophie Halliez [d], Bert Brône [c], Frédéric Saudou [e], Laurence Ris [b], Sylvain Gabriele [a,*]

[a] Mechanobiology & Biomaterials Group, CIRMAP, Research Institute for Biosciences, University of Mons, B-7000, Mons, Belgium
[b] Neuroscience Laboratory, Neuroscience Department, Research Institute for Biosciences, University of Mons, B-7000, Mons, Belgium
[c] Neurophysiology Laboratory, BIOMED Research Institute, UHasselt, B-3500, Hasselt, Belgium
[d] Univ. Lille, Inserm, CHU Lille, U1172 - LilNCog - Lille Neuroscience & Cognition, F-59000, Lille, France
[e] Univ. Grenoble Alpes, Inserm, U1216, CHU Grenoble Alpes, Grenoble Institut Neuroscience, F-38000, Grenoble, France

ARTICLE INFO

Keywords:
Microglia
Stretching assay
Mechanical injury
Activation
DNA damages
Synapse stripping

ABSTRACT

Microglial cells, as the primary defense line in the central nervous system, play a crucial role in responding to various mechanical signals that can trigger their activation. Despite extensive research on the impact of chemical signaling on brain cells, the understanding of mechanical signaling in microglia remains limited. To bridge this gap, we subjected microglial cells to a singular mechanical stretch and compared their responses with those induced by lipopolysaccharide treatment, a well-established chemical activator. Here we show that stretching microglial cells leads to their activation, highlighting their significant mechanosensitivity. Stretched microglial cells exhibited distinct features, including elevated levels of Iba1 protein, a denser actin cytoskeleton, and increased persistence in migration. Unlike LPS-treated microglial cells, the secretory profile of chemokines and cytokines remained largely unchanged in response to stretching, except for TNF-α. Intriguingly, a single stretch injury resulted in more compacted chromatin and DNA damage, suggesting potential long-term genomic instabilities in stretched microglia. Using compartmentalized microfluidic chambers with neuronal networks, we observed that stretched microglial cells exhibited enhanced phagocytic and synaptic stripping activities. These findings collectively suggest that stretching events can unlock the immune potential of microglial cells, contributing to the maintenance of brain tissue homeostasis following mechanical injury.

1. Introduction

Throughout a lifetime, the human body is continually subjected to various forces. In certain pathological scenario, brain tissue can experience a rapid load, leading to substantial internal stress and the application of stretching and compressive forces [1]. The inflammatory response ensuing from these mechanical insults is recognized as a significant secondary injury mechanism, carrying potential long-term consequences such as an elevated risk of developing neurodegenerative disorders, chronic traumatic encephalopathy, and amyotrophic lateral sclerosis in later stages of life [2]. In this neuroinflammatory context, glial cells play a crucial role in producing inflammatory mediators, scavenging cellular debris and orchestrating neurorestorative processes to facilitate neurological recovery. Microglia, among glial cells, are the immune resident cells of the brain and perform essential functions in antigen presentation [3], phagocytosis [4], programmed cell death [5], vessel patterning [6] and neuronal plasticity, including synaptic pruning [7]. Under normal physiological conditions, microglia assume a monitoring state, extending their processes to scan the microenvironment for potential threats, contributing to the maintenance of neuronal networks by releasing minimal amount of cytokines and chemokines, and eliminating cellular debris and unnecessary synapses through phagocytosis [8]. During traumatic events and inflammatory episodes, microglial cells transition to a reactive mode, enabling them to orchestrate an immune response against disturbances in central nervous system (CNS) homeostasis. Depending on the nature of changes in stimuli, microglia can adopt different activation states characterized by altered morphology, gene expression, and function. It has been demonstrated that microglia respond to various chemical factors, such as lipopolysaccharides (LPS) or interferon-gamma (IFN-γ), triggering a

* Corresponding author.
E-mail address: sylvain.gabriele@umons.ac.be (S. Gabriele).

https://doi.org/10.1016/j.biomaterials.2023.122426
Received 14 May 2023; Received in revised form 29 November 2023; Accepted 8 December 2023
Available online 15 December 2023

reactive state [9]. Surprisingly, it was shown that microglia can remain in an activated state for days, weeks, and even years following trauma [10,11]. However, despite recent advances in understanding the mechanosensitivity of microglial cells [12,13], the mechanisms and functional consequences of a mechanically activated microglial cells remain unclear.

A more comprehensive understanding of the mechanobiological aspects of traumatic brain injury (TBI) is crucial for advancing the field. In this study, we aimed to explore the impact of mechanical injury on microglial cells. To simulate traumatic mechanical stress, we subjected microglial cells cultured on deformable elastomer membranes to a uniaxial stretch of 20 % of strain. Mechanically-activated microglial cells were then compared to LPS-activated microglial cells to gain further insights in the mechanisms and functional consequences of a mechanical injury.

2. Results

2.1. Single stretch of microglial cells results in their activation

To simulate traumatic mechanical stress, we subjected BV2 cells — a type of cortical microglial cell derived from C57/BL6 mice [14] — to a uniaxial stretch. BV2 microglial cells were cultured on polydimethylsiloxane (PDMS) chambers coated with a mix of laminin and poly-L-lysine to ensure a specific engagement of transmembrane integrins. After 24 h in culture, BV2 cells underwent a single uniaxial stretch of 20 % in less than a second (Fig. 1A and Supplementary Movie S1). The behavior of mechanically activated microglial cells was compared to a chemical activation with lipopolysaccharides (LPS), a widely used pro-inflammatory stimulus for microglia *in vitro* and *in vivo* [15-17]. While LPS-treated cells may not fully represent the spectrum of activated microglial cells following TBI, they provide a benchmark for comparing mechanically-activated microglial cells to a well-known pro-inflammatory scenario [18].

Supplementary data related to this article can be found online at https://doi.org/10.1016/j.biomaterials.2023.122426

We initially assessed the state of activation of microglial cells by immunostaining the ionized calcium-binding adapter molecule (Iba1), specifically more expressed in activated microglia and macrophages [19]. Our findings revealed that mechanically-activated and LPS-treated microglial cells exhibited increased Iba1 protein fluorescence intensity compared to the control group (Fig. 1B-C), demonstrating that a 20 % stretch injury can induce a reactive phenotype of microglial cells without causing additional cell death (Supplementary Fig. 1).

Considering Iba1 as an actin cross-linker, we hypothesized that the mechanical activation of microglia induces the reorganization of their actin cytoskeleton. Notably, stretched and LPS-treated cells exhibited higher F-actin fluorescence intensity compared to the control group (Fig. 1D-E), suggesting that the mechanical activation of microglial cells strengthens their actin cytoskeleton. Similar experiments on primary mouse microglial cells (PMCs) demonstrated a consistent linear relation between fluorescence signals of Iba1 and actin (Supplementary Fig. 2), validating our results obtained on BV2 microglial cells.

Building upon the modulation of the actin cytoskeleton and its cross-linker Iba1 in stretch-injured microglia, we characterized their elastic modulus using a nanoindenter operating in liquid mode at 37 °C (Fig. 1F and Supplementary Movie S2). Our findings indicated that control microglial cells were very soft with an elastic modulus of 51.1 ± 2.2 Pa, in agreement with previous reports [20]. In contrast, we observed a stiffening of LPS-treated and stretched microglia with elastic moduli of 68.9 ± 2.9 Pa and 63.2 ± 2.9 Pa, respectively. Interestingly, we identified a linear relation ($R^2 = 0.9888$) between the cell stiffness and the actin fluorescence intensity (Fig. 1 G).

Supplementary data related to this article can be found online at https://doi.org/10.1016/j.biomaterials.2023.122426

2.2. Secretion of most pro-inflammatory chemokines and cytokines in microglial cells is not affected by stretch injury, except for TNF-α

Microglial activation leads to the production of pro-inflammatory cytokines such as IL-1β, IFN-γ, and TNF-α [21]. While these factors are released to prevent further damages to CNS tissues, they may also exert toxic effects to neurons and glial cells [22]. Activated microglia can adopt diverse states with different surface receptors, intracellular markers, secreted factors, and functions. Given that both LPS-treated and stretched microglial cells enter an activated state, we characterized their secretory profile to gain insights into the phenotype associated with mechanical injury.

We conducted Mesoscale Discovery (MSD) electrochemiluminescence multiplex immunoassays to analyze the concentration of IFN-γ, IL-1β, IL-2, IL-5, IL-6, IL-10, IL-12p70, KC/GRO, and TNF-α in the supernatant of untreated, LPS-treated and mechanically-activated microglial cells. As shown in Fig. 2A, our results indicated that 7 cytokines (IFN-γ, IL-2, IL-6, IL-10, IL-12p70, KC/GRO, and TNF-α) were significantly more secreted by LPS-activated cells compared to untreated microglia, with IFN-γ and IL-1β remained unaffected (Fig. 2B). Notably, the concentration of KC/GRO showed a tendency to increase in stretched microglial cell media (Fig. 2C), although it did not reach statistical significance ($p = 0.4675$). Moreover, the concentration of TNF-α increased in the culture medium of LPS-treated (28732 ± 1149 pg/ml) and, to a lesser extent, in mechanically-activated microglia (4025 ± 1283 pg/ml) compared to healthy microglia (2590 ± 953 pg/ml) (Fig. 2D). In contrast to LPS-treated cells, these results demonstrate that mechanical stretch can activate Iba-1 in microglia without significantly altering the secretory profile of most chemokines and cytokines, except for TNF-α. The secretion of cytokines by activated microglial cells can vary depending on the trigger for cell activation [18], highlighting the multifaceted nature of activated microglial cells. In our previous work, we showed that TNF-α secreted by stretched astrocytes plays a key role in synaptic loss in neuronal networks, suggesting a complex interplay between mechanically injured glial cells [23].

2.3. Mechanical activation induces a more persistent migration

While accumulating evidence suggests that the transition between a surveilling and a reactive mode in microglia induces a modulation of their morphology and migratory behavior [9], the impact of a mechanical injury on these properties of microglial cells remains unclear. To address this question, we assessed the morphological and dynamic characteristics of BV2 cells through time-lapse microscopy experiments by using CellTracker, a live fluorescent dye. Our findings revealed that BV2 cells exhibited a larger perimeter (100.9 ± 36.7 μm) and spreading area (500.1 ± 180.1 μm^2) in response to LPS treatments. Additionally, confocal imaging demonstrated that LPS-treated BV2 cells had a larger cellular volume (7049 ± 3342 μm^3) than control cells (2080 ± 1140 μm^3). Mechanically-activated BV2 cells were characterized by a larger spreading area (407.4 ± 179 μm^2, Fig. 3A) and a larger perimeter (92.4 ± 40.4 μm, Fig. 3B) than control cells. However, we did not observe significant modifications of the cellular volume (3101 ± 1491 μm^3) in mechanically-activated cells (Fig. 3C).

Considering that a stretch injury induces a strengthening of the actin cytoskeleton and recruitment of Iba1, which interacts with RAC GTPases participating in lamellipodial protrusion via the ARP2/3 complex [24], we aimed to probe the migratory behavior of mechanically-activated microglial cells. We studied the migration of BV2 microglial cells for 15 h using protein microstripes of 15 μm wide to standardize our migration assays (Supplementary Movie S3). Time-lapse microscopy with live fluorescent labelling of the nucleus (Fig. 3D-E) was used to track cell displacement over time (Fig. 3F and Supplementary Movie S4). Our results showed that control microglial cells had a mean velocity of 0.40 ± 0.12 μm/min, whereas LPS-treated and mechanically-activated microglial cells were slightly faster (0.47 ± 0.09 μm/min and 0.46 ±

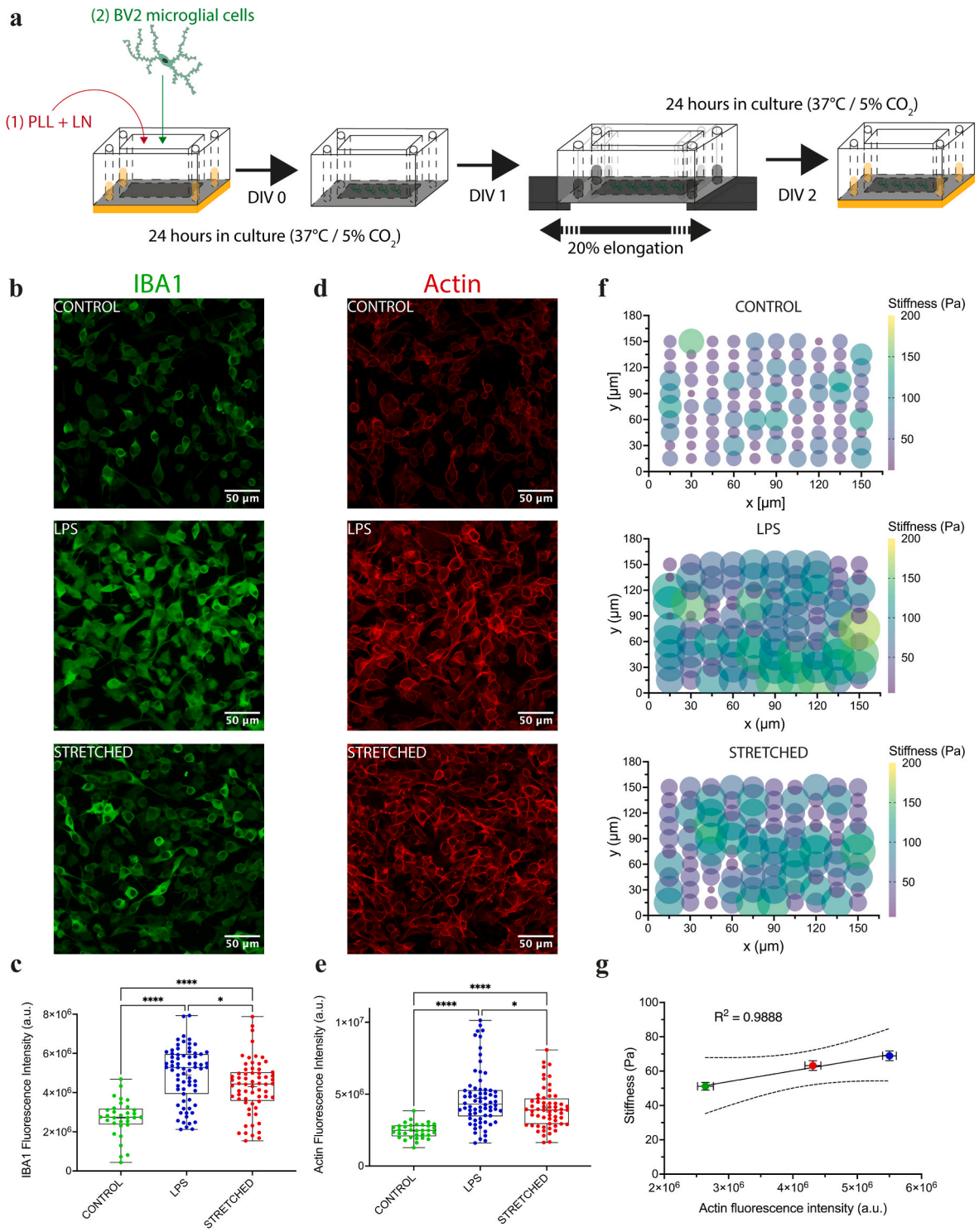

Fig. 1. Single stretch of microglial cells results in their activation. (A) BV2 cells were cultured for 24 h on deformable chambers coated with poly-L-lysine and laminin (PLL/LA). A deformable chamber was placed on an automatic stretcher and subjected to a uniaxial stretch of 20 % elongation in less than a second. Stretched chambers were then maintained at 37 °C and 5 % CO_2 for 24 h. (B) Immunostaining of Iba1 in microglial cells without treatment (control), chemically activated with LPS at 100 ng/ml for 24 h (LPS) and mechanically activated with a 20 % stretch (stretched). (C) Total fluorescence intensity for Iba1 in the control group (n = 32), LPS (n = 71), and stretched (n = 64). (D) Immunostaining of F-actin in microglial cells for control, LPS, and stretched cells (E) Total fluorescence intensity for Iba1 in control group (n = 33), LPS (n = 70), and stretched (n = 59). (F) Cell stiffness probed with a nanoindenter as a function of (*x*,*y*) spatial coordinates for the control (n = 99), LPS (n = 120), and stretched (n = 109) groups. (G) Linear relation between the stiffness of microglial cells in function of the actin fluorescence intensity (R^2 = 0.9888). N = 3 replicates for the control and N = 6 replicates for LPS and stretched groups. Scale bars are 50 µm ns ≥ 0.05, 0.01 ≤ p* ≤ 0.05, 0.001 ≤ p** ≤ 0.01, p*** ≤ 0.001.

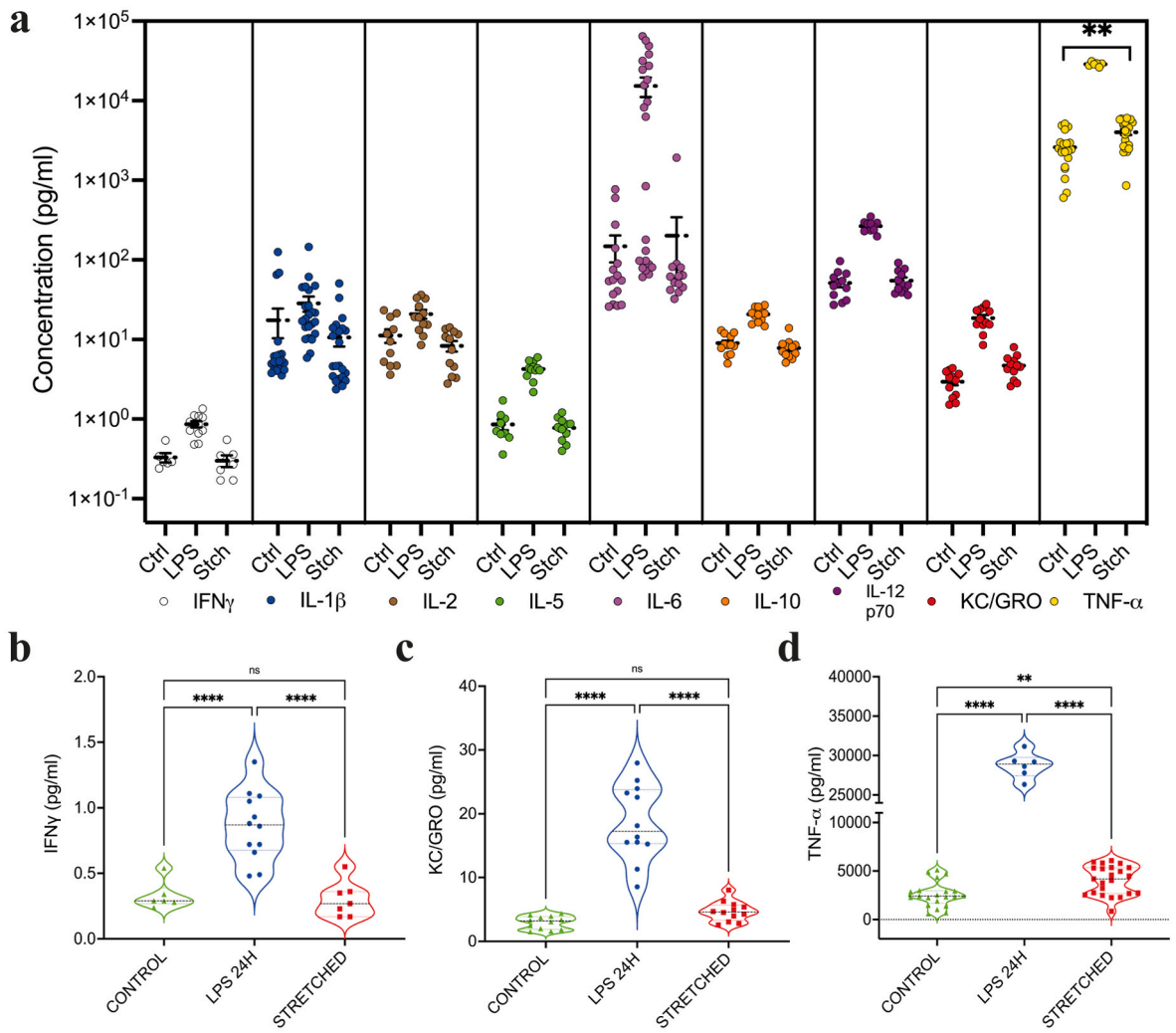

Fig. 2. Secretion of most pro-inflammatory chemokines and cytokines in microglial cells is not affected by a stretch injury, except for TNF-α. (A) Nested plots showing the concentration of nine cyto-chemokines (IFN-γ, IL-1β, IL-2, IL-5, IL-6, IL-10, IL-12p70, KC/GRO, and TNF-α) in the media of healthy, LPS-treated, and mechanically-activated microglial cells. (B) Concentration of IFN-γ (control: n = 6; LPS: n = 6; stretched: n = 6). (C) Concentration of KC-GRO (control: n = 6; LPS: n = 6; stretched: n = 6). (D) Concentration of TNF-α (control: n = 11; LPS: n = 6; stretched: n = 12). ns is not significant, 0.01 ≤ p* ≤ 0.05, 0.001 ≤ p** ≤ 0.01, p*** ≤ 0.001.

0.15 μm/min, respectively) (Fig. 3G-H). Additionally, LPS-treated and mechanically-activated BV2 cells exhibited fewer direction changes (41 ± 7.8 and 50 ± 6.4, respectively) than control cells (61 ± 11.4) (Fig. 3I). These results suggest that activated microglial cells adopt a more persistent mode of migration, with fewer back-and-forth movements, leading to more efficient goal-directed migration (Supplementary Fig. 4).

Supplementary data related to this article can be found online at https://doi.org/10.1016/j.biomaterials.2023.122426

2.4. Stretch injury induces chromatin compaction and DNA damage

During their migration within in the cerebral parenchyma, microglial cells undergo important deformations to navigate in narrow spaces. As the largest and stiffest organelle in eukaryotic cells [25], the nucleus is constantly subjected to intrinsic and extrinsic forces, leading to various nuclear deformations [26], which contribute to cellular perception of mechanical stimuli [27,28]. The nucleus is not only the primary site of gene replication and transcription but also a fundamental mechanotransduction component, capable of mechanosensing and orchestrating key cellular functions in response to mechanical stimulation [26].

To understand whether a single stretch of 20 % can affect the nuclear integrity of microglial cells, we immunostained the nucleus with diamidino-2-phenylindole (DAPI), which selectively bind to the minor groove of double-stranded DNA. Using 3D confocal images, we observed that nuclear volume of mechanically-activated microglial cells (957 ± 274 μm^3) was larger than that of control (424.5 ± 109.8 μm^3) and LPS-treated (543.3 ± 195.8 μm^3) cells (Supplementary Fig. 3), suggesting that mechanical activation of microglia leads to elevated nuclear influx accompanied by nuclear volume expansion.

We then assessed whether the influx of cytoplasmic constituents could affect condensation state of the chromatin [29,30]. As shown in Fig. 4A-B, our results indicated that mechanically-activated microglial cells exhibited larger domains of chromatin compaction (0.15 ± 0.04 a.u.) than control (0.07 ± 0.03 a.u.) and LPS-treated (0.08 ± 0.02 a.u.) cells. These results suggest that a single 20 % stretch induces more condensed chromatin states, potentially affecting gene expression, while chromatin organization is not affected by a chemical activation with LPS treatment. To delve further, we used immunocytochemical assays to study the potential presence of the phosphorylated form of γH2Ax (Fig. 4C), resulting from double-strand breaks [31]. As shown in Fig. 4D, we found a substantial increase of the number of γH2Ax foci in mechanically-activated microglia nuclei (25.9 ± 20 foci), indicating

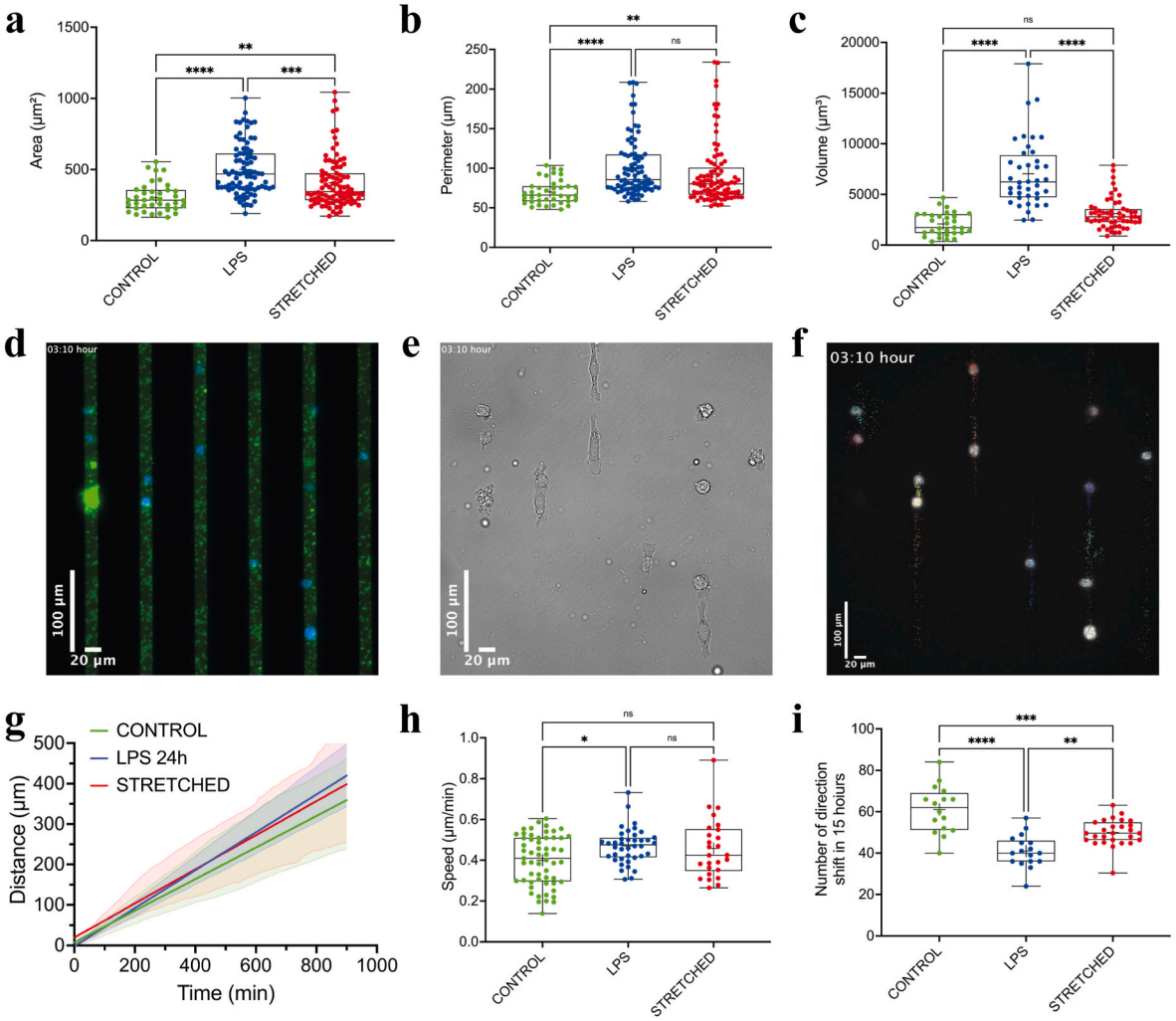

Fig. 3. Mechanically-activated microglial cells are larger and more persistent. (A) Spreading area, (B) perimeter and (C) cellular volume for control (n = 39, in green), LPS-treated cells (n = 85, in blue), and stretched cells (n = 91, in red). Typical images of microglial cells migrating (D) on PLL-LA microstripes of 15 µm width (green) and (E) observed in Differential Interferential Contrast (DIC) mode. (F) The nucleus stained with DAPI (in blue) for automatic tracking on time-lapse experiments of 15 h with a frame rate of 10 min. (G) Temporal evolution of the travelled distance and (H) average migration speed for control (n = 58, in green), LPS-treated cells (n = 40, in blue), and stretched cells (n = 26, in red). (I) Number of direction shifts for control (n = 16, in green), LPS-treated cells (n = 17, in blue), and stretched cells (n = 26, in red). Scale bars are 20 µm ns is not significant, $0.01 \leq p^* \leq 0.05$, $0.001 \leq p^{**} \leq 0.01$, $p^{***} \leq 0.001$. (For interpretation of the references to color in this figure legend, the reader is referred to the Web version of this article.)

that many DNA breaks occur in response to a stretch injury (Supplementary Movie S5). The number of foci was statistically similar between the control group (10.8 ± 7.6 foci) and the LPS group (14.2 ± 10.4 foci) (Fig. 4D).

Supplementary data related to this article can be found online at https://doi.org/10.1016/j.biomaterials.2023.122426

Based on these results, we then investigated the mechanical sensitivity of chemically and mechanically activated microglial cells to 3D confined migration. To this aim, we performed transmigration assays through a porous membrane with pores of 8 µm in diameter (Fig. 4E). No differences in the number of nuclear foci were observed between transmigrated and control cells (Fig. 4F), suggesting that a transmigration through a porous membrane does not induce additional DNA defects. Furthermore, LPS-treated or mechanically-activated microglial cells did not exhibit any additional γH2Ax foci after transmigration (Fig. 4G). Overall, these results demonstrated that transmigration through 3D confined spaces does not lead to severe nuclear deformations and thus DNA damages, in contrast to a 20 % stretch injury, suggesting different impacts on nuclear integrity between endogenous stress during confined migration and exogenous stress during tissue stretching.

2.5. *Phagocytosis and synaptic stripping are enhanced in stretch injured microglia*

As the resident macrophages of the brain tissues, microglia play a crucial role in antigen presentation and clearing cellular debris or pathogens threatening brain homeostasis. Phagocytosis, the process by which a cell recognizes, engulfs and digests a target that is ≥ 1 µm in size, including dead or dying cells, is a vital function of microglial cells during both physiological and pathological conditions [32,33]. To assess the phagocytotic capacity of microglial cells, we introduced pre-opsonized fluorescent latex beads into the culture medium for 1 h and then we washed away the excess beads, counting only those that had been phagocytized using 3D confocal images (Fig. 5A). We observed a 3-fold increase of the phagocytic activity in mechanically-activated microglial cells (1.5 ± 0.4 beads/cell), while there was a slight augmentation in LPS-treated cells (0.9 ± 0.5 bead/cell) compared to the control group (0.6 ± 0.3 bead/cell) (Fig. 5B).

Building on our previous results, we were wondering whether

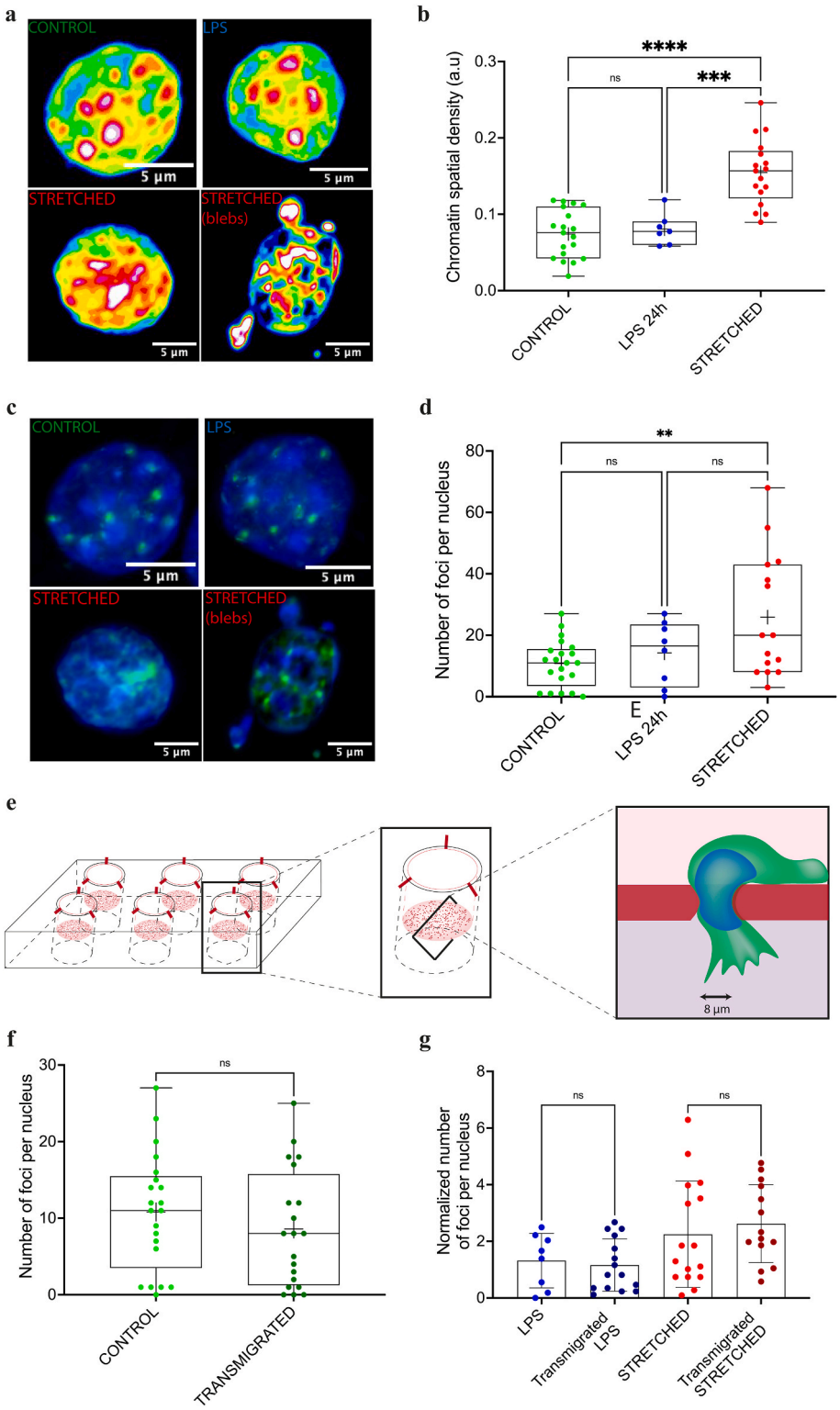

Fig. 4. Stretch injury results in more compacted chromatin and DNA damage, whereas confined transmigration does not. (A) Typical confocal images of nuclei with the fluorescence intensity of DAPI digitized (0-255 bits) and color coded (from high to low: white, purple, red, orange, yellow, green, light blue and dark blue). Highly condensed domains show higher fluorescence intensity with respect to the less condensed ones. (B) Average chromatin spatial densities of control (n = 19, in blue), LPS-treated cells (n = 7, in green), and stretched cells (n = 17, in red). (C) Typical confocal images of immunostained nuclei for DAPI (in blue) and γH2Ax foci (in green). (D) Number of foci per nucleus for control (n = 23, in blue), LPS-treated cells (n = 7, in green), and stretched cells (n = 17, in red). (E) Schematic representation of a transwell migration assay. Microglial cells were seeded on a culture insert with a porous membrane of Teflon (pores of 8 µm in diameter) placed inside a 6-well plate. The culture insert was filled with a serum-free medium (light pink), and a complete medium was placed in the well of the plate (dark pink). The serum gradient triggers the confined transmigration of microglial cells through the narrow pores. (F) Number of foci per nucleus of control (n = 23, light green) and transmigrated control cells (n = 7, dark green). (G) Normalized number of foci per nucleus control for control and transmigrated LPS-treated and stretched cells. ns is not significant, $0.01 \leq p^{*} \leq 0.05$, $0.001 \leq p^{**} \leq 0.01$, $p^{***} \leq 0.001$. (For interpretation of the references to color in this figure legend, the reader is referred to the Web version of this article.)

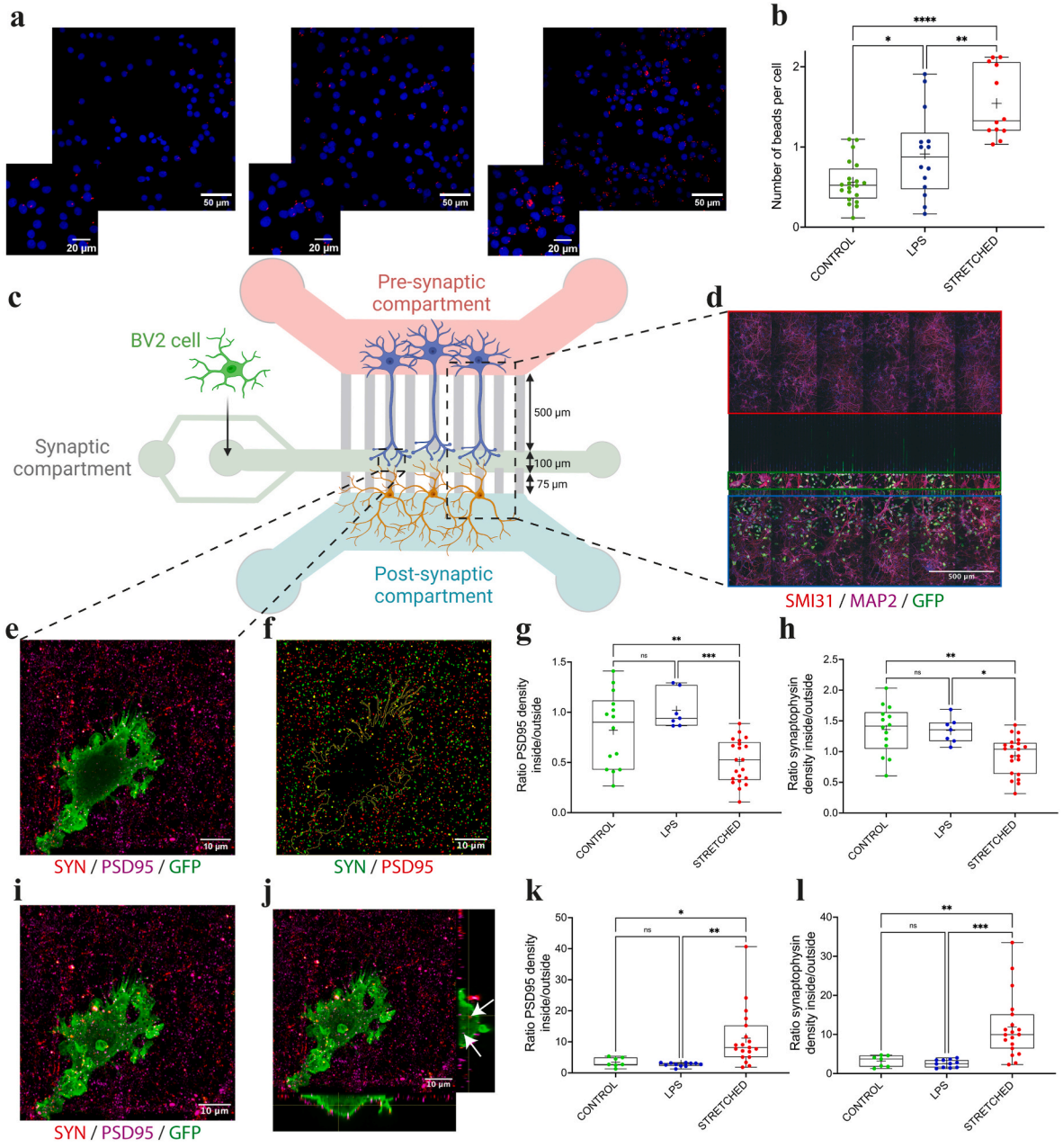

Fig. 5. Mechanical activation of microglial cells triggers increased phagocytosis and synaptic stripping activities. (A) Confocal images of nuclei (stained with DAPI in blue) and fluorescent latex beads (in red) in microglial cells. (B) Mean number of beads per cell for control (n = 20, in green), LPS-treated (n = 14, in blue), and stretched cells (n = 12, in red), with N ≥ 3 replicates. (C) Schematic representation of the microfluidic chamber. Primary cortical neurons were seeded in pre-synaptic (in light red) and post-synaptic (light blue) chambers. BV2 cells were seeded in the synaptic compartment (light green) at neuronal network DIV10. (D) Typical confocal image of the microfluidic chamber immunostained for SMI31 (red), MAP2 (purple), and GFP (green). GFP-BV2 microglial cells migrated to synapses and through lower and upper channels (3 µm wide). (E) Confocal image (3 µm-depth) of microglial cells immunostained for synaptophysin (red), PSD95 (purple) and GFP (green). (F) Processed image showing the microglial cell contour (yellow line) and pixelized dots for synaptophysin (green) and PSD95 (red). Ratio between inside and outside microglial cell densities for (G) PSD95 and (H) synaptophysin for control (n = 14, in green), LPS-treated (n = 7, in blue) and stretched cells (n = 21, in red). (I) Confocal image of a microglial cell immunostained for synaptophysin (red), PSD95 (purple) and GFP (green). (J) Orthogonal views of the confocal image showing the presence of synaptophysin (red) and PSD95 (purple) dots inside the cell (white arrows). Ratio between inside and outside microglial cell densities for (K) PSD95 and (L) synaptophysin for control (n = 7), LPS (n = 11) and stretched cells (n = 19), without the first 3 µm of confocal acquisition. ns ≥ 0.05, 0.01 ≤ p* ≤ 0.05, 0.001 ≤ p** ≤ 0.01, p*** ≤ 0.001. (For interpretation of the references to color in this figure legend, the reader is referred to the Web version of this article.)

mechanical activation of microglial cells could modulate synapses in neuronal networks, particularly during synaptic stripping. To study synaptic stripping in a physiologically relevant system, we utilized microfluidic devices that allow to reconstitute *in vitro* mature cortico-cortical networks [34-36]. The microfluidic device comprises presynaptic and postsynaptic compartments containing cortical neurons. An intermediate synaptic compartment receives axons from presynaptic cortical neurons and dendrites from post-synaptic cortical neurons. The three compartments are connected by 3-µm-wide microchannels, with axons (500 µm long) and dendrites (75 µm long) (Fig. 5C). Because the axonal channels are 500 µm long, only axons from the cortex can reach the synaptic compartment. A laminin gradient from the pre-synaptic chamber to the post-synaptic chamber limits the number of post-synaptic axons that can reach the synaptic chamber (Fig. 5C).

Microglial cells labelled with a GFP-encoding lentivirus were introduced into the synaptic compartment, allowing the study of co-culture stained for GFP, dendritic microtubule-associated protein 2 (MAP2), and an axonal phosphorylated neurofilament H (SMI31) marker (Fig. 5D) at DIV10. At this stage, functional maturity of the circuit is achieved [35,36]. Pre-synaptic cortical neurons have established functional excitatory connections to post-synaptic cortical neurons and pre-treated GFP-microglial cells were introduced into the synaptic compartments. All microfluidic experiments were performed from DIV10 to DIV11 for cortico-cortical neuronal networks and 24 h after chemical and mechanical treatments of GFP-microglial cells.

We stained synaptic compartments with antibodies recognizing pre-synaptic protein synaptophysin (SYN) and the postsynaptic density protein 95 (PSD95). We acquired confocal Z-stacks images of 3 μm depth representing the entire layer of synaptic connections into the synaptic compartment. Images were were acquired at different zones and acquisitions of different areas containing at least one GFP-microglia and pre- and post-synaptic proteins labelled were used for quantifications (Supplementary Movie S6). Images were first thresholded to remove non-specific signals and then the number of synaptophysin and PSD-95 spots were counted automatically by using the Analyze Particle plugin in FIJI [37]. Inside and outside areas were delimited by masks of the contour of microglial cells (Fig. 5E-F). The ratio between inside and outside post-synaptic dot density (PSD-95) was significantly lower in mechanically-activated microglial cells (0.5 ± 0.2) than in LPS-treated (1.0 ± 0.2) and control (0.8 ± 0.3) cells (Fig. 5G). Similar results were observed for the ratio between inside and outside pre-synaptic dot density (synaptophysin), significantly decreased in mechanically-activated microglial cells (0.9 ± 0.3) compared to LPS-treated (1.3 ± 0.2) and control (1.4 ± 0.4) cells. These findings suggest that stretch injured-microglial exhibit enhanced stripping activity.

To confirm these results, we performed confocal z-stack images in high-resolution mode of microglial cells (Supplementary Movie S7). After subtracting a basal focal plane of 3 μm thickness, corresponding to the mean thickness of the synapses resting in the synaptic compartment (Fig. 5I and Supplementary Movie S8), we observed synaptic proteins only localized within the microglial cells (Fig. 5J). Comparing the ratio between inside and outside synaptophysin and PSD95 dot density, we found a higher PSD95 protein dot ratio in mechanically-activated microglial cells (11.2 ± 9.3) than in LPS-activated (2.7 ± 0.6) and control (3.4 ± 1.5) cells (Fig. 5K-L). Additionally, our results showed a higher synaptophysin protein dot ratio in mechanically-activated microglial cells (11.9 ± 8.1) than in LPS-activated (2.6 ± 3) and healthy cells (3.1 ± 1.5).

Altogether, these results demonstrate that, unlike LPS treatment, a single mechanical stretch on microglial cells induces an enhanced synaptic stripping activity on healthy neuronal networks. Considering that microglial cells can remain *in vivo* in an activated state for very long periods, our findings are crucial for a better understanding of the remodeling of the neuronal connectivity after a traumatic event.

Supplementary data related to this article can be found online at https://doi.org/10.1016/j.biomaterials.2023.122426

3. Discussion

Brain injuries are complex and heterogeneous pathologies involving numerous factors. Microglial cells, rapidly activated after a brain injury, release signals that collectively inititate an inflammatory cascade in brain tissues. Peripheral immune cells can be recruited within minutes following injury [38]. In this study, we demonstrate that microglial cells are mechanosensitive and undergo changes in morphology, cytoskeleton, and phagocytic activity in response to stretching deformation, resembling events during brain injury.

A brief and moderate stretch deformation induces a reactive state characterized by elevated Iba1 levels. Unlike LPS-activated microglial cells, stretched cells do not secrete a wide range of pro-inflammatory cytokines. Notably, our findings reveal that stretch injury induces the secretion of pro-inflammatory cytokines, with TNF-α being the only cytokine affected. TNF-α, known to influence synaptic scaling, post-synaptic current frequency, and synaptic plasticity, suggests a distinct microglial activation state in response to chemical or mechanical stimuli, hinting at different underlying pathways [39-41].

In addition to important differences in the secretory profile, stretch injuries result in abundant double-strand DNA breaks, which does not impact DNA integrity. Intriguingly, confined migration of microglial cells in narrow spaces does not induce DNA damages, indicating the ability of microglia to discern between endogenously induced mechanical stress during migration and exogenously induced stress during short, mild injuries.

Phagocytosis, integral to microglial innate immune responses and adaptive contributions to antigen presentation [42], is enhanced by mechanical injury. This is often considered beneficial for tissue homeostasis, rapidly clearing dying cells and preventing the release of proinflammatory and neurotoxic molecules [43]. However, different targets and related receptors can finely tune microglia responses, which appear as a continuum of activation states [44]. For instance, phagocytosis of apoptotic neurons mediated by microglial triggering receptor expressed on myeloid cells-2 (TREM-2) is associated with decreased pro-inflammatory cytokines production [45], while myelin debris phagocytosis enhances pro-inflammatory and dampens the anti-inflammatory profile in microglia [46].

Our evidence suggests that mechanically-activated microglia can remove damaged cells and strip synapses from neurons. Activation of microglia in response to stretch injury may protect neurons by removing inhibitory synapses. Further studies are needed to distinguish the phagocytic role of activated microglia in removing dying cells from their neuroprotective role in stripping synapses. Deciphering the molecular signature for protective microglia and understanding the duration and reversibility of neuroprotection provided by mechanically-activated microglia are essential areas for further investigation. Studying whether neurons can instruct activated microglia to transition from a neuroprotective to a phagocytic phenotype is also an intriguing avenue for future exploration.

4. Conclusion

Microglial are responsive cells exhibiting distinct reactions and adaptions to chemical and mechanical treatments in different ways. The mechanical activation of microglial cells emerges as a pivotal stage in the context of neuroinflammation and synaptic stripping during the hours and days following the lesion. These collective findings suggest a potential role for activated microglia in enhancing neuromodulation within injured brains. Future research endeavors should explore how alterations in chromatin compaction and DNA damage in stretched microglia might contribute to genomic instabilities. Despite recognition of the integrin (α5β1)/FAK pathway as a significant contributor to stretched microglial responses [47], the mechanotransduction mechanism triggering morphological changes, chromatin compaction and enhanced stripping activity remain poorly understood. Our study reveals an augmentation of phagocytic activity [48] in mechanically-activated microglia plated on laminin-coated substrates, while other reports did not observe significant differences in stripping activity when mechanically-activated microglia where cultured on fibronectin. These results hint at a potential role for integrin signaling in the mechanical activation of microglial cells, consistent with previous works on diffuse axonal injury (DAI) in cortical neurons [49]. Further investigations are essential to pinpoint the exact molecular pathway involved in the mechanical activation process of microglia, offering potential avenues for developing therapeutic strategies for preventing long-term disabilities following brain trauma.

5. Experimental section

Preparation of cell culture substrates. To replicate the mechanical deformations observed during TBI events, we designed stretchable chambers using a thin polydimethylsiloxane (PDMS) membrane, increasingly recognized for the fabrication of neuronal cell culture platforms and microfluidic devices [50,51]. The PDMS curing agent (Dow Corning, Sylgard 184) was mixed with a base agent in a mass ratio of 12:1 in 15 mL centrifugal tubes. After placing the mixture in a vacuum for 30 min to eliminate air bubbles, it was transferred onto a silanized Teflon mold. Subsequently, the PDMS mixture underwent spin-coating (POLOS Wafer Spinner) with a speed gradually increasing from 100 to 600 rpm over 30 s, followed by curing at 60 °C for 4 h. The resulting PDMS layer reached a thickness of 150 μm. This PDMS membrane was fixed to a PDMS block, forming a stretchable chamber. To assess the field deformation of the elastic PDMS membranes, fluorescent protein (FITC-BSA) circles of 2000 μm^2 were printed on the device's membrane. The device underwent uniaxial 20 % stretching along the horizontal axis, and the distances between the centers of the circles were determined along both horizontal and vertical axes [23].

Fabrication of microfluidic devices. The construction of polydimethylsiloxane (PDMS) microfluidic devices follows a well-documented design [34-36]. Initially, a master mold was created with SU-8 photoresist on a silicon wafer through a dual thickness photolithography process. The microfluidic circuit consists of a network of thin, slender microchannels connecting three larger culture chambers: *pre-synaptic*, *post-synaptic* and synaptic, as illustrated in Ref. [36]. Epoxy resins (master replica of the 3 inches processed silicon wafers) were used to fill the PDMS mixture into the molds, and the removal of air bubbles were achieved by placing the mold in a desiccator under vacuum for 1 h. Subsequently, polymerization occurred by incubating the PDMS for 3 h at 60 °C. The resulting PDMS microchambers were then cut, washed with 100 % ethanol, subjected to a quick ultrasonic bath, and finally rinsed with distilled water. The cut PDMS pieces and glass-bottom Petri dishes (FluoroDish, WPI, 0.17 μm-thick and 35 mmin diameter) underwent surface activation in a plasma cleaner under vacuum for 30 s. After a rapid passage in an oven at 60 °C, the PDMS pieces and Petri dishes were meticulously joined to create an irreversible, airtight seal. For optimal functionality, the microfluidic devices were coated with a mixture of poly-D-lysine (0.1 mg/ml) in the upper and synaptic chambers. Additionally, the lower chamber was coated with a mix of poly-D-lysine (0.1 mg/ml) and laminin (10 μg/ml) overnight at 4 °C. To ensure cleanliness and viability, microchambers of microfluidic channels underwent 3 washes with a growth medium (Neurobasal medium supplemented with 2 % B27, 2 mM Glutamax, and 1 % penicillin/streptomycin) and were then prewarmed at 37 °C before neurons were introduced.

Cell culture and chemical/mechanical treatments. Microglial cells derived from the BV2 cell line (BV2, Elabscience, EP-CL-0493) were cultured and maintained in polystyrene T75 flasks within a cell culture incubator at 37 °C with 5 % CO_2. The BV2 cells were cultured in a proliferation medium consisting of Dulbecco's modified Eagle's medium, high glucose (4.5 g/L) with L-glutamine (BE12-604F, Lonza). This medium was further supplemented with 10 % (v/v) fetal bovine serum (FBS; AE Scientific), and 1 % penicillin and streptomycin antibiotics (AE Scientific). For all experimental groups, BV2 cells were seeded on stretched chamber of 10^3 cells per chamber. Chemical and mechanical treatments (LPS and stretch) were initiated 24 h after seeding, and all experiments were conducted 24 h after treatment, equating to 48 h post-seeding. For chemical activation of microglial cells, Lipopolysaccharides from *Escherichia coli* (LPS) were utilized at a concentration of 100 ng/ml (Sigma-Aldrich, L4516-1 MG). A single mechanical injury, mimicking the deformations observed during traumatic brain injury, was induced by a 20 % stretch. Stretching experiments were conducted using an automatic stretcher (StrexCell STB-150) (Fig. 3A). To ensure the stability of the chambers during manipulation and prevent undesired deformations, a custom-made stabilizer was created through 3D printing (Ulti Maker V1.9), reinforcing the structure of the stretchable chamber. This stabilizer not only enhanced structural integrity but also prevented any unintended deformations during the handling of the deformable chambers.

Isolation and culture of primary microglial cells. Cortical microglia from $CX3CR1^{eGFP/+}$ WT mice were isolated following established procedures [52]. In brief, brains of post-natal day 21 (P21) mice were dissected, with careful removal of the midbrain, cerebellum and meninges. The remained tissue was immersed in Dulbecco's Modified Eagle's Medium (DMEM, Sigma-Aldrich, Overijse, Belgium) supplemented with 1 % penicillin/streptomycin (P/S, Invitrogen, Merelbeke, Belgium). Papain (17 U/mg, Sigma-Aldrich) and DNase I (10 mg/ml, Roche, Brussel, Belgium) were used for enzymatic digestion for 30 min at 37 °C. The resulting cell suspensions were filtered through a 70 μm cell strainer, centrifuged (5 min, 500 g), and pellets were resuspended in DMEM containing 30 % stock isotonic Percoll (SIP, GE Healthcare, Diegem, Belgium). A density gradient was established by adding of 70 % SIP diluted in PBS, followed by centrifugation for 25 min at 650 g (brake 0, acceleration 4). The cell cloud at the interphase between 30 % and 70 % was collected, diluted in 10 ml cold PBS, and centrifuged for 10 min at 500 g. Cell pellets were resuspended in magnetic activated cell sorting (MACS) buffer (2 mM EDTA and 0.5 % fetal calf serum (FCS)). Microglia were isolated by positive selection using CD11b microbeads (Miltenyi Biotec, Gladbach, Germany), following the manufacturer's instructions. $CD11b^+$ cells were then resuspended in DMEM supplemented with 10 % FCS, 10 % horse serum (Thermofisher, Waltham, MA, US) and 1 % P/S (DMEM 10:10:1) before seeded onto stretchable chambers (30 x 10^3 cells/well). The chambers pre-coated with poly-D-lysine (PDL, 20 μg/ml, Gibco, Waltham, MA, US) and collagen type IV (2 μg/ml, Sigma - Aldrich), and cells were incubated in a humidified incubator at 37 °C and 5 % CO_2 for 7 days. Afterwards, a dynamic ramified morphology was induced by the addition of serum-free medium (hereafter referred as TIC medium) containing 5 μg/ml insulin, 5 μg/ml N-acetyl-cysteine, 100 μg/ml apo-transferrin, 0.1 μg/ml Na_2SeO_3, 1 μg/ml heparan sulfate, 2 μg/ml human TGF-β (PeproTech, Rocky Hill, NJ, US), 0.1 μg/ml murine IL-34 (BioL egend, Amsterdam, The Netherlands), 1.5 μg/ml ovine wool cholesterol, 3 μg/ml L-glutamine in DMEM/F12. For all experiments, cells were initially seeded 7 days in DMEM 10:10:1 medium followed by 3-7 days TIC medium before the commencement of experiments.

Primary rat cortical neurons cultures. Primary cortical neurons were cultured following established protocols [53]. Cortex dissection from E15.5 wild-type (Wistar-Han) rat embryos was performed, and the tissue was digested using a papain and cysteine solution. Subsequently, two incubations with trypsin inhibitor solutions were carried out, and the tissue was finally mechanically dissociated. Dissociated cortical neurons were resuspended in growing medium ($5x10^6$ cells in 80 μl) and plated in the chamber with a final density of ~7000 cells/mm^2. Cortical neurons were initially plated in the pre-synaptic chamber, followed by the addition of cortical neurons in the post-synaptic chamber. After an incubation period of at least 1 h, all compartments were gently filled with growing medium. Prior to experiments, microchambers were carefully inspected to prevent any cell contamination in the synaptic chamber.

Lentiviruses. BV2 microglial cells were infected at DIV1 with lentiviruses (LV) for 72 h and then washed with growing medium. Cultures expressing at least 80 % of the plasmid were then plated in stretchable chambers. The LV construct used for the study was pSIN-EF1α-eGFP.

Indentation and measurements protocol. Microglial cells stiffness was assessed using the Chiaro indenter system (Optics11, Amsterdam, the Netherlands). This system consists of a ferrule-top force transducer [54], comprising a micromachined cantilever spring with an optical fiber readout, mounted on a 3D-printed holder screwed to a Z-piezoelectric actuator (PI p-603.5S2, Physik Instrumente). The single-mode fiber of the readout was coupled to an interferometer (OP1550, Optics11), where the interference signal was directly translated into cantilever

deflection. The piezoelectric actuator with the probe was mounted on a XYZ micromanipulator (PatchStar, Scientifica) for the automatic mapping of mechanical properties. Indentation mapping was performed in parallel lines, with at least 25 (5X x 5Y) points per chamber. The distance between two adjacent locations were 15 μm to ensure sufficient separation between indentation areas. Colloidal probes with a tip diameter of 3 μm were employed to test the microglial cells stiffness. Three samples were tested for each condition, resulting in total of 110-126 indentation data points recorded per experimental group. Before testing, the sensitivity calibration of the cantilever was conducted by indenting a hard glass surface. The Hertz model was applied to fit an initial loading data up to the cantilever threshold value to obtain the true surface position:

$$F = \frac{4}{3}\frac{E}{1-\nu^2}\frac{R}{\sqrt{h^3}}$$

where F is the load, E is an elastic modulus, v is the Poisson's ratio of compressibility (we assume that brain cells are incompressible v = 0.5), h is the indentation depth.

Immunostaining in stretchable and microfluidic chambers. BV2 cells were fixed and permeabilized using a solution containing 4 % paraformaldehyde (Electron Microscopy Sciences) and 0.05 % Triton X-100 (Sigma) in PBS (1X, Capricorn Scientific) for 15 min at room temperature (RT). Following fixation, cells were rinsed three times with warm PBS and incubated for 30 min in a blocking solution containing 1 % BSA (GE Healthcare) and 5 % FBS in PBS. BV2 cells were labelled for F-actin using Alexa Fluor 555 phalloidin (1:200; Invitrogen A34055), DNA with DAPI (1:200; Thermo Fisher Scientific, D1306), and Iba1 (1:750) Sopachem, 019-19741). γH2Ax was labelled with anti-phospho histone H2A.X (Ser139), coupled to Alexa Fluor 488 conjugate antibody monoclonal antibody (1:200; Millipore Sigma, clone JBW301: 05-636-AF488) for 1 h at RT. The PDMS membranes with immunostained cells were cut off the stretch chamber and mounted on microscope slides using slow-fade diamond antifade (Thermo Fisher, Molecular Probes) for epifluorescence and confocal imaging. For neurons in the microchambers, fixation was carried out with a PFA/Sucrose solution (4 %/4 % in PBS) for 20 min at RT. After rinsing the fixation buffer three times with PBS, neurons were incubated for 1h at RT in a blocking solution (BSA 1 %, normal goat serum 2 %, Triton X-100 0.1 %). The region of interest was then incubated with primary antibodies overnight at 4 °C, and appropriate fluorescent secondary antibodies were applied for 1 h at RT. Immunofluorescence was stored in PBS for a maximum of one week in the dark at 4 °C. The primary antibodies used were: PSD95 (Millipore, MAB1598, 1:1000), Synaptophysin (Abcam, AB14692, 1:200), MAP2 (Chemicon, AB5622, 1:500), GFP (Abcam, Ab13970, 1:2000).

Cytokine quantification. To quantify the amount of inflammatory cytokines and chemokines released by control, LPS-treated and mechanically-activated BV2 microglial cells, a Meso Scale Discovery (MSD) electrochemiluminescence multiplex immunoassay (Meso Scale Diagnostics, Maryland, US) was employed. The V-PLEX Plus Proinflammatory Panel1 Mouse Kit, K15048G-1) allowed the quantification of interferon gamma (IFN-γ); interleukins 2, 4, 5, 6, 10, 12p70, and 1β (IL-4, IL-5, IL-6, Il-10, and IL-1β); tumour necrosis factor alpha (TNF-α) and the chemokine KC/GRO also known as CXCL1, even at a very low concentration (lowest LLOD is 0.65 pg/ml for the IFN-γ). This multi-array technology combines electrochemiluminescence and multi-spot plates to enable precise quantitation of multiple analytes in a single sample, requiring less time and effort than other assay platforms. The assay can be considered as a "sandwich immunoassay" with a 96-well 10 spot-plate pre-coated with capture antibodies.

Migration assays. Microglial cells were subjected to chemical or mechanical treatment in stretchable chambers and trypsinized 24 h post-treatment. Cells were seeded on PDMS-coated fluorodish that were microprinted with mixture of Poly-L-Lysine and Laminine (PLL-LA) microstripes, each 15 μm wide. After minimum 4 h for cell spreading, the fluorodishes were placed under a microscope at 37 °C with 5 % CO_2. Images were taken every 10 min for 15 h, and time-lapse sequences were analyzed with FIJI and the Cell Tracker code on MatLab to determine the migration speed and the persistence time.

Phagocytosis assay. Microglial cells, treated either chemically (LPS) or mechanically (stretch) in stretchable chambers, were subjected to a phagocytosis assay. After 24 h post-treatment, a controlled number (10 beads/cell) of fluorescent latex beads with a diameter of 1 μm of diameter (Sigma-Aldrich, L2778-1 ML) were introduced in the medium for 1 h. The medium was then removed to eliminate non-phagocytosed beads, and cells were fixed with PFA for 15 min. Following immunostaining, images were captured using a confocal microscope in at least 3 different regions of interest (ROIs) per sample.

Synaptophysin and PSD95 analysis. Colocalization and independent dots analyses of synaptophysin and PSD95 were conducted using ImageJ. Airyscan images were thresholded to eliminate non-specific signals. The number of synaptophysin spots overlapping, juxtaposed, or separated by no more than 2 pixels (130 nm) to PSD95 spots were counted automatically. Results were expressed as a function of density outside the area of microglial cells and the density inside. Each condition was tested using at least 3 chambers per culture from 3 independent cultures. In each chamber, 3 fields were analyzed, and 3 regions of interest were selected.

Epifluorescence, confocal and time-lapse imaging. Immunostained preparations of BV2 cells were examined in epifluorescence and confocal modes using a Nikon A1R HD25 (Nikon, Japan) motorized inverted microscope equipped with × 20, × 40 and × 60 Plan Apo (numerical aperture, 1.45; oil immersion) objectives. Lasers covering the violet (405 and 440 nm), blue (457, 477 and 488 nm), green (514 and 543 nm), yellow-orange (568 and 594 nm) and red (633 and 647 nm) spectral regions were employed. Epifluorescence images were recorded with a Prime 95B camera (Photometrics) using NIS-Elements Advanced Research 4.5 software (Nikon). Z-stack images were collected using either a × 60 or × 40 objective for three channels (DAPI, TRITC and FITC) from the entire volume of the nuclei using a step size of 0.15 μm or the cell using a step size of 1 μm. Exposure times and laser power were kept constant, and the acquired stack of images was deconvolved to eliminate focus light. PSD95/SYN immunostaining was acquired in the synaptic chamber with a × 63 oil-immersion objective (1.4 NA) using an inverted confocal microscope (LSM 710, Zeiss) coupled to an Airyscan detector, enhancing signal-to-noise ratio and spatial resolution. Time-lapse experiments were conducted at 37 °C and 5 % CO_2 for 15 h on a Nikon A1R HD25 (Nikon, Japan) motorized inverted microscope, equipped with a cage incubator (OkoLab) and controlled with the NIS Elements Advanced Research 4.0 software (Nikon, Japan).

Image analysis. All images were acquired with NIS-Elements Advanced Research software (v.4.5, Nikon, Japan) under consistent illumination and recording conditions (camera frequency, gain and lamp intensity). Quantification of Iba1 and actin fluorescence intensity was performed using a corrected total fluorescence intensities analysis method. For each image, area, raw integrated density, mean grey value, and the number of cells were measured. Additionally, five random background regions were selected to obtain a mean grey value of the fluorescent background [55]. The corrected total fluorescence was calculated using the following equation:

$$PF_C = ID_R - (MO_A - MF_B)$$

with PF_C as the corrected protein fluorescence intensity, ID_R the raw integrated density, MO_A the marked objects area and MF_B the mean fluorescence background. Images were captured in a minimum of 3 different regions of interest (ROI) for each sample obtained from 6 distinct chambers (n = ROIs). Confocal images were processed using FIJI software [37].

Statistical analysis. Experimental data were presented through

boxplots, multiple-variable graphs, or histograms. Statistical comparisons were realized by either a Student t-test or ANOVA, where ns $\geq$ 0.05, 0.01 $\leq$ p* $\leq$0.05, 0.001 $\leq$ p** $\leq$0.01, p*** $\leq$0.001.

Ethical compliance. Experiments involving mice were carried out in strict accordance with the European Community guiding principles on the care and use of animals. The study received approval from the Ethical Committee on Animal Research of Hasselt University (Project license 201956K). Animals were group-housed in a controlled environment with regulated temperature and humidity, provided with *ad libitum* access to food and water, and maintained on a 12 h light-dark cycle. The CX3CR1$^{eGFP/+}$ strain was obtained by breeding CX3CR1$^{eGFP/GFP}$ with wild type C57BL6 mice. CX3CR1$^{eGFP/GFP}$ mice [56] were sourced from the European Mouse Mutant Archive (EMMA) Institute, with the approval of Steffen Jung (Weizmann Institute of Science).

CRediT authorship contribution statement

Anthony Procès: Conceptualization, Investigation, Methodology, Resources, Validation, Writing - original draft, Writing - review & editing. **Yeranddy A. Alpizar:** Methodology, Resources, Writing - review & editing. **Sophie Halliez:** Methodology, Writing - review & editing. **Bert Brône:** Methodology, Resources, Writing - review & editing. **Frédéric Saudou:** Methodology, Resources, Validation, Writing - review & editing. **Laurence Ris:** Funding acquisition, Methodology, Supervision, Writing - review & editing. **Sylvain Gabriele:** Conceptualization, Funding acquisition, Methodology, Resources, Supervision, Validation, Writing - original draft, Writing - review & editing.

Declaration of competing interest

The authors declare the following financial interests/personal relationships which may be considered as potential competing interests: Sylvain Gabriele reports financial support was provided by University of Mons. Anthony Proces reports financial support was provided by Fund for Scientific Research. Yeranddy A. Alpizar reports financial support was provided by Research Foundation Flanders. Frederic Saudou reports financial support was provided by European Research Council.

Data availability

Data will be made available on request.

Acknowledgements

The authors thank Djamal Achour from the IMPact de l'Environnement Chimique sur la Santé (ULR 4483 - IMPECS) team for his help with the quantification of cytokines and Johanna Cormenier for her help with microfluidic experiments. A.P. and S.G. acknowledges funding from FEDER Prostem Research Project no. 1510614 (Wallonia DG06), the F.R.S.-FNRS Epiforce Project no. T.0092.21, the F.R.S.-FNRS CellSqueezer Project no. J.0061.23, the F.R.S.-FNRS Optopattern Project no. U.NO26.22 and the Interreg MAT(T)ISSE project, which is financially supported by Interreg France-Wallonie-Vlaanderen (Fonds Européen de Développement Régional, FEDER-ERDF). Y.A.A was supported by an FWO senior postdoctoral fellowship (12H8220 N). Y.A.A. and B.B. are supported by the BOF small research project 21KP06BOF. F.S. acknowledges funding from European Research Council (ERC) under the European Union's Horizon 2020 research and innovation programme AdG grant agreement no. 834317, Fueling Tranport. We acknowledge Yasmina Saoudi and the Photonic Imaging Center of Grenoble Institute Neuroscience (Univ Grenoble Alpes - Inserm U1216) which is part of the ISdV core facility and certified by the IBiSA label. A.P. is financially supported by F.R.S.-FNRS with a FRIA PhD grant and Fonds pour la Recherche Médicale en Hainaut (FRMH). L.R. and S.G. thank Programme Wallon d'Investissement Région Wallone pour les instruments d'imagerie (INSTIMAG UMONS #1910169).

Appendix A. Supplementary data

Supplementary data to this article can be found online at https://doi.org/10.1016/j.biomaterials.2023.122426.

References

[1] W.J. Tyler, The mechanobiology of brain function, Nat. Rev. Neurosci. 13 (12) (2012) 867–878.
[2] R. Gupta, N. Sen, Traumatic brain injury: a risk factor for neurodegenerative diseases, Rev. Neurosci. 27 (1) (2016) 93–100.
[3] E.N. Goddery, C.E. Fain, C.G. Lipovsky, K. Ayasoufi, L.T. Yokanovich, C.S. Malo, R. H. Khadka, Z.P. Tritz, F. Jin, M.J. Hansen, A.J. Johnson, Microglia and perivascular macrophages act as antigen presenting cells to promote CD8 T cell infiltration of the brain, Front. Immunol. 12 (2021), 726421.
[4] E. Janda, L. Boi, A.R. Carta, Microglial phagocytosis and its regulation: a therapeutic target in Parkinson's disease? Front. Mol. Neurosci. 11 (2018) 144.
[5] J.L. Marín-Teva, I. Dusart, C. Colin, A. Gervais, N. van Rooijen, M. Mallat, Microglia promote the death of developing purkinje cells, Neuron 41 (4) (2004) 535–547.
[6] S.K. Halder, R. Milner, A critical role for microglia in maintaining vascular integrity in the hypoxic spinal cord, Proc. Natl. Acad. Sci. U.S.A. 116 (51) (2019) 26029–26037.
[7] R.C. Paolicelli, G. Bolasco, F. Pagani, L. Maggi, M. Scianni, P. Panzanelli, M. Giustetto, T.A. Ferreira, E. Guiducci, L. Dumas, D. Ragozzino, C.T. Gross, Synaptic pruning by microglia is necessary for normal brain development, Science 333 (6048) (2011) 1456–1458.
[8] S.M.-T. Smolders, S. Kessels, T. Vangansewinkel, J.-M. Rigo, P. Legendre, B. Brône, Microglia: brain cells on the move, Prog. Neurobiol. 178 (2019), 101612.
[9] A.M. Jurga, M. Paleczna, K.Z. Kuter, Overview of general and discriminating markers of differential microglia phenotypes, Front. Cell. Neurosci. 14 (2020) 198.
[10] D.J. Loane, A. Kumar, B.A. Stoica, R. Cabatbat, A.I. Faden, Progressive neurodegeneration after experimental brain trauma: association with chronic microglial activation, J. Neuropathol. Exp. Neurol. 73 (1) (2014) 14–29.
[11] C. Smith, Review: the long-term consequences of microglial activation following acute traumatic brain injury: neuroinflammation after trauma, Neuropathol. Appl. Neurobiol. 39 (1) (2013) 35–44.
[12] Y.-B. Lu, K. Franze, G. Seifert, C. Steinhauser, F. Kirchhoff, H. Wolburg, J. Guck, P. Janmey, E.-Q. Wei, J. Kas, A. Reichenbach, Viscoelastic properties of individual glial cells and neurons in the CNS, Proc. Natl. Acad. Sci. USA 103 (47) (2006) 17759–17764.
[13] L. Bollmann, D.E. Koser, R. Shahapure, H.O.B. Gautier, G.A. Holzapfel, G. Scarcelli, M.C. Gather, E. Ulbricht, K. Franze, Microglia mechanics: immune activation alters traction forces and durotaxis, Front. Cell. Neurosci. 9 (2015).
[14] A. Henn, The suitability of BV2 cells as alternative model system for primary microglia cultures or for animal experiments examining brain inflammation, ALTEX (2009) 83–94.
[15] Y. Wang, G. Jin, H. Miao, J.Y.-S. Li, S. Usami, S. Chien, Integrins regulate VE-cadherin and catenins: dependence of this regulation on Src, but not on Ras, Proc. Natl. Acad. Sci. USA 103 (6) (2006) 1774–1779.
[16] I.C.M. Hoogland, C. Houbolt, D.J. van Westerloo, W.A. van Gool, D. van de Beek, Systemic inflammation and microglial activation: systematic review of animal experiments, J. Neuroinflammation 12 (1) (2015) 114.
[17] S. Lund, K.V. Christensen, M. Hedtjärn, A.L. Mortensen, H. Hagberg, J. Falsig, H. Hasseldam, A. Schrattenholz, P. Pörzgen, M. Leist, The dynamics of the LPS triggered inflammatory response of murine microglia under different culture and in vivo conditions, J. Neuroimmunol. 180 (1-2) (2006) 71–87.
[18] S. Lively, L.C. Schlichter, Microglia responses to pro-inflammatory stimuli (LPS, IFNγ+TNFα) and reprogramming by resolving cytokines (IL-4, IL-10), Front. Cell. Neurosci. 12 (2018) 215.
[19] Y. Sasaki, K. Ohsawa, H. Kanazawa, S. Kohsaka, Y. Imai, Iba1 is an actin-cross-linking protein in macrophages/microglia, Biochem. Biophys. Res. Commun. 286 (2) (2001) 292–297.
[20] J. Rheinlaender, A. Dimitracopoulos, B. Wallmeyer, N.M. Kronenberg, K.J. Chalut, M.C. Gather, T. Betz, G. Charras, K. Franze, Cortical cell stiffness is independent of substrate mechanics, Nat. Mater. 19 (9) (2020) 1019–1025.
[21] E.C. Beattie, D. Stellwagen, W. Morishita, J.C. Bresnahan, B.K. Ha, M. Von Zastrow, M.S. Beattie, R.C. Malenka, Control of synaptic strength by glial TNFα, Science 295 (5563) (2002) 2282–2285.
[22] L. Henning, H. Antony, A. Breuer, J. Müller, G. Seifert, E. Audinat, P. Singh, F. Brosseron, M.T. Heneka, C. Steinhäuser, P. Bedner, Reactive microglia are the major source of tumor necrosis factor alpha and contribute to astrocyte dysfunction and acute seizures in experimental temporal lobe epilepsy, Glia 71 (2) (2023) 168–186.
[23] J. Lantoine, A. Procès, A. Villers, S. Halliez, L. Buée, L. Ris, S. Gabriele, Inflammatory molecules released by mechanically injured astrocytes trigger presynaptic loss in cortical neuronal networks, ACS Chem. Neurosci. 12 (20) (2021) 3885–3897.
[24] M. Schaks, G. Giannone, K. Rottner, Actin dynamics in cell migration, Essays Biochem. 63 (5) (2019) 483–495.
[25] J. Lammerding, Mechanics of the nucleus, in: *Comprehensive Physiology*, 1ed, Wiley, 2011, pp. 783–807.

[26] Y. Kalukula, A.D. Stephens, J. Lammerding, S. Gabriele, Mechanics and functional consequences of nuclear deformations, Nat. Rev. Mol. Cell Biol. 23 (9) (2022) 583–602.
[27] S.E. Szczesny, R.L. Mauck, The nuclear option: evidence implicating the cell nucleus in mechanotransduction, J. Biomech. Eng. 139 (2) (2017).
[28] J.T. Long, J. Lammerding, Nuclear deformation lets cells gauge their physical confinement, Dev. Cell 56 (2) (2021) 156–158.
[29] M. Luciano, S.-L. Xue, W.H. De Vos, L. Redondo-Morata, M. Surin, F. Lafont, E. Hannezo, S. Gabriele, Cell monolayers sense curvature by exploiting active mechanics and nuclear mechanoadaptation, Nat. Phys. 17 (12) (2021) 1382–1390.
[30] M. Versaevel, T. Grevesse, S. Gabriele, Spatial coordination between cell and nuclear shape within micropatterned endothelial cells, Nat. Commun. 3 (1) (2012) 671.
[31] L.J. Kuo, L.-X. Yang, Gamma-H2AX - a novel biomarker for DNA double-strand breaks 22 (3) (2008) 305–309.
[32] A. Hochreiter-Hufford, K.S. Ravichandran, Clearing the dead: apoptotic cell sensing, recognition, engulfment, and digestion, Cold Spring Harbor Perspect. Biol. 5 (1) (2013) a008748-a008748.
[33] G.C. Brown, J.J. Neher, Microglial phagocytosis of live neurons, Nat. Rev. Neurosci. 15 (4) (2014) 209–216.
[34] C. Scaramuzzino, E.C. Cuoc, P. Pla, S. Humbert, F. Saudou, Calcineurin and huntingtin form a calcium-sensing machinery that directs neurotrophic signals to the nucleus, Sci. Adv. 8 (1) (2022), eabj8812.
[35] E. Moutaux, W. Christaller, C. Scaramuzzino, A. Genoux, B. Charlot, M. Cazorla, F. Saudou, Neuronal network maturation differently affects secretory vesicles and mitochondria transport in axons, Sci. Rep. 8 (1) (2018), 13429.
[36] A. Virlogeux, E. Moutaux, W. Christaller, A. Genoux, J. Bruyère, E. Fino, B. Charlot, M. Cazorla, F. Saudou, Reconstituting corticostriatal network on-a-Chip reveals the contribution of the presynaptic compartment to huntington's disease, Cell Rep. 22 (1) (2018) 110–122.
[37] J. Schindelin, I. Arganda-Carreras, E. Frise, V. Kaynig, M. Longair, T. Pietzsch, S. Preibisch, C. Rueden, S. Saalfeld, B. Schmid, J.-Y. Tinevez, D.J. White, V. Hartenstein, K. Eliceiri, P. Tomancak, A. Cardona, Fiji: an open-source platform for biological-image analysis, Nat. Methods 9 (7) (2012) 676–682.
[38] K.N. Corps, T.L. Roth, D.B. McGavern, Inflammation and neuroprotection in traumatic brain injury, JAMA Neurol. 72 (3) (2015) 355.
[39] O. Pascual, S. Ben Achour, P. Rostaing, A. Triller, A. Bessis, Microglia activation triggers astrocyte-mediated modulation of excitatory neurotransmission, Proc. Natl. Acad. Sci. U.S.A. 109 (4) (2012).
[40] P.T. Nguyen, L.C. Dorman, S. Pan, I.D. Vainchtein, R.T. Han, H. Nakao-Inoue, S. E. Taloma, J.J. Barron, A.B. Molofsky, M.A. Kheirbek, A.V. Molofsky, Microglial remodeling of the extracellular matrix promotes synapse plasticity, Cell 182 (2) (2020) 388–403.e15.
[41] A.K. Clark, D. Gruber-Schoffnegger, R. Drdla-Schutting, K.J. Gerhold, M. Malcangio, J. Sandkuhler, Selective activation of microglia facilitates synaptic strength, J. Neurosci. 35 (11) (2015) 4552–4570.
[42] G.W. Litman, J.P. Cannon, J.P. Rast, New insights into alternative mechanisms of immune receptor diversification, in: Advances in Immunology vol. 87, Elsevier, 2005, pp. 209–236.
[43] S.A. Wolf, H.W.G.M. Boddeke, H. Kettenmann, Microglia in physiology and disease, Annu. Rev. Physiol. 79 (1) (2017) 619–643.
[44] U.-K. Hanisch, H. Kettenmann, Microglia: active sensor and versatile effector cells in the normal and pathologic brain, Nat. Neurosci. 10 (11) (2007) 1387–1394.
[45] K. Takahashi, C.D.P. Rochford, H. Neumann, Clearance of apoptotic neurons without inflammation by microglial triggering receptor expressed on myeloid cells-2, J. Exp. Med. 201 (4) (2005) 647–657.
[46] T.A. Siddiqui, S. Lively, L.C. Schlichter, Complex molecular and functional outcomes of single versus sequential cytokine stimulation of rat microglia, J. Neuroinflammation 13 (1) (2016) 66.
[47] M.C. Shaughness, N. Pierron, A.N. Smith, K.R. Byrnes, The integrin pathway partially mediates stretch-induced deficits in primary rat microglia, Mol. Neurobiol. 60 (6) (2023) 3396–3412.
[48] M. Shaughness, K. Byrnes, Assessment of the effects of stretch-injury on primary rat microglia, Mol. Neurobiol. 58 (7) (2021) 3545–3560.
[49] M.A. Hemphill, B.E. Dabiri, S. Gabriele, L. Kerscher, C. Franck, J.A. Goss, P. W. Alford, K.K. Parker, A possible role for integrin signaling in diffuse axonal injury, PLoS One 6 (7) (2011), e22899.
[50] T. Grevesse, B.E. Dabiri, K.K. Parker, S. Gabriele, Opposite rheological properties of neuronal microcompartments predict axonal vulnerability in brain injury, Sci. Rep. 5 (1) (2015).
[51] J. Lantoine, T. Grevesse, A. Villers, G. Delhaye, C. Mestdagh, M. Versaevel, D. Mohammed, C. Bruyère, L. Alaimo, S.P. Lacour, L. Ris, S. Gabriele, Matrix stiffness modulates formation and activity of neuronal networks of controlled architectures, Biomaterials 89 (2016) 14–24.
[52] J. Beeken, M. Mertens, N. Stas, S. Kessels, L. Aerts, B. Janssen, F. Mussen, S. Pinto, R. Vennekens, J.-M. Rigo, L. Nguyen, B. Brône, Y.A. Alpizar, Acute inhibition of transient receptor potential vanilloid-type 4 cation channel halts cytoskeletal dynamism in microglia, Glia 70 (11) (2022) 2157–2168.
[53] G. Liot, D. Zala, P. Pla, G. Mottet, M. Piel, F. Saudou, Mutant huntingtin alters retrograde transport of TrkB receptors in striatal dendrites, J. Neurosci. 33 (15) (2013) 6298–6309.
[54] D. Chavan, T.C. van de Watering, G. Gruca, J.H. Rector, K. Heeck, M. Slaman, D. Iannuzzi, Ferrule-top nanoindenter: an optomechanical fiber sensor for nanoindentation, Rev. Sci. Instrum. 83 (11) (2012), 115110.
[55] T. Corne, T. Sieprath, J. Vandenbussche, Deregulation of focal adhesion formation and cytoskeletal tension due to loss of A-type lamins, Cell Adhes. Migrat. 11 (2017) 447–463.
[56] S. Jung, J. Aliberti, P. Graemmel, M.J. Sunshine, G.W. Kreutzberg, A. Sher, D. R. Littman, Analysis of fractalkine receptor CX(3)CR1 function by targeted deletion and green fluorescent protein reporter gene insertion, Mol. Cell Biol. 20 (11) (2000) 4106–4114.